Editors' Suggestion

Observation of a pressure-induced transition from interlayer ferromagnetism to intralayer antiferromagnetism in $Sr_4Ru_3O_{10}$

H. Zheng,[1] W. H. Song,[1,2] J. Terzic,[3] H. D. Zhao,[1] Y. Zhang,[1] Y. F. Ni,[1] L. E. DeLong,[4] P. Schlottmann,[5] and G. Cao[1,*]

[1]*Department of Physics, University of Colorado at Boulder, Boulder, Colorado 80309, USA*
[2]*Institute of Solid State Physics, Chinese Academy of Sciences, Hefei 230031, China*
[3]*National High Magnetic Field Laboratory, Tallahassee, Florida 32306, USA*
[4]*Department of Physics and Astronomy, University of Kentucky, Lexington, Kentucky 40506, USA*
[5]*Department of Physics, Florida State University, Tallahassee, Florida 32306, USA*

(Received 21 June 2018; revised manuscript received 3 August 2018; published 21 August 2018)

$Sr_4Ru_3O_{10}$ is a Ruddlesden-Popper compound with triple Ru-O perovskite layers separated by Sr-O rock-salt layers. This compound presents a rare coexistence of interlayer (c-axis) ferromagnetism and intralayer (basal-plane) metamagnetism at ambient pressure. Here we report the observation of pressure-induced, intralayer *itinerant antiferromagnetism* arising from the interlayer ferromagnetism. The application of modest hydrostatic pressure generates an anisotropy that may cause a flattening and a tilting of RuO_6 octahedra. All magnetic and transport results from this study indicate these lattice distortions diminish the c-axis ferromagnetism and basal-plane metamagnetism, and induce a basal-plane antiferromagnetic state. The unusually large magnetoelastic coupling and pressure tunability of $Sr_4Ru_3O_{10}$ makes it a model system for studies of itinerant magnetism.

DOI: 10.1103/PhysRevB.98.064418

I. INTRODUCTION

$Sr_4Ru_3O_{10}$ is a "triple-layer" member of the Ruddlesden-Popper ruthenates, $(Ca, Sr)_{n+1}Ru_nO_{3n+1}$ (n = number of Ru-O perovskite layers per unit cell). Ruthenates feature extended $4d$-electron orbitals and comparable energy scales (and therefore competition) among Coulomb interactions, crystalline electric fields (CEF), spin-orbit interactions, p-d hybridization, and spin-lattice coupling. The deformations and relative orientations of corner-shared RuO_6 octahedra determine the CEF level splitting and the electronic band structure, and hence the ground state. Consequently, the physical properties of ruthenates are highly sensitive to dimensionality and susceptible to perturbations such as the application of magnetic field, and/or pressure. These characteristics are well demonstrated by the contrasting physical properties of $Ca_{n+1}Ru_nO_{3n+1}$ and $Sr_{n+1}Ru_nO_{3n+1}$ ($n = 1, 2, 3, \infty$). The Ca-based compounds are on the verge of a metal-insulator transition and prone to antiferromagnetism (AFM) whose character changes with n. In contrast, the Sr-based compounds are metallic and evolve from paramagnetism ($n = 1, 2$) to ferromagnetism (FM) ($n = \infty$) with increasing n [1–20]. It is therefore not surprising that these materials exhibit nearly every cooperative phase known in solids.

The triple-layered $Sr_4Ru_3O_{10}$ ($n = 3$) [12] is precariously positioned on the borderline separating the ferromagnet $SrRuO_3$ ($n = \infty$) [5] and the field-induced metamagnet $Sr_3Ru_2O_7$ ($n = 2$) [9,10], and displays complex phenomena ranging from tunneling magnetoresistance and quantum oscillations [21] to a switching effect [15]. However, the most distinct, intriguing hallmark of $Sr_4Ru_3O_{10}$ is its seemingly contradictory magnetic behavior: for an external magnetic field applied *along the c axis* (perpendicular to the layers), it exhibits itinerant FM with a Curie temperature $T_C = 105$ K and a saturation moment greater than $1.0\,\mu_B$/Ru [Fig. 1(a)]; on the other hand, when the magnetic field is applied *within the basal plane* it features a pronounced peak in the magnetization near $T_M = 50$ K [Fig. 1(a)] and a sharp metamagnetic transition near $H_c = 2.5$ T [Fig. 1(b)] [12,21–23]. This situation recalls the metamagnetic transitions out of Stoner exchange-enhanced paramagnetism in Sr-based Ruddlesden-Popper compounds [24–27]. The coexistence of the interlayer FM and the intralayer metamagnetism is not anticipated from simple theoretical arguments [24,25,28]. A two-dimensional, tight-binding electron gas has a logarithmic divergence in the density of states which, depending on the position of the Fermi level, can yield FM, metamagnetism, and a quantum critical point by varying applied pressure [29]. However, $Sr_4Ru_3O_{10}$ is not strictly two-dimensional and a suitable model must be adapted accordingly, whereupon $Sr_4Ru_3O_{10}$ then provides an opportunity to study the interplay of itinerant FM, AFM, and metamagnetism.

The peculiar behavior of $Sr_4Ru_3O_{10}$ ($n = 3$) has drawn considerable attention in recent years [23,30–33]. Discussions have mainly focused on the relationship between the interlayer FM and the intralayer metamagnetism below T_M, the onset of the metamagnetic state. A Raman study explores the spin-lattice coupling as a function of temperature, magnetic field, and pressure, and informs a microscopic description of structural and magnetic phases [14]. Specifically, magnetic-field-induced changes in the phonon spectra reveal spin-reorientation transitions and strong magnetoelastic coupling below T_M [14]. Neutron-scattering studies [34,35] indicate a collinear FM state aligned along the c axis with no detectable spin canting toward the basal plane. The

*gang.cao@colorado.edu

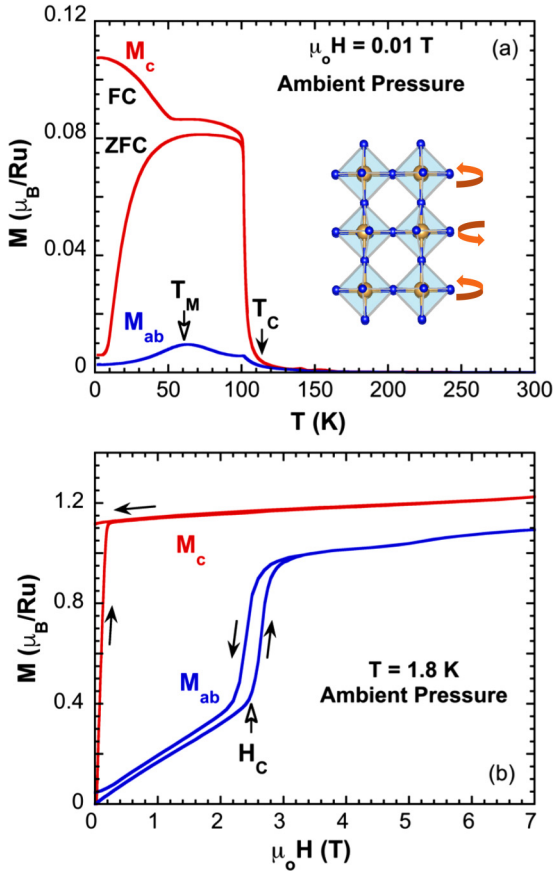

FIG. 1. (a) Temperature dependence of the magnetization M at $\mu_o H = 0.01$ T, and (b) isothermal magnetization $M(H)$ at $T = 1.8$ K for both the basal-plane M_{ab} and the c-axis M_c at ambient pressure. Inset: Schematic of the triple-layered crystal structure; the curved arrows indicate the rotation of the RuO_6 octahedra. Note that the data in this figure, which was from our earlier work [21], were taken at ambient pressure without the pressure cell, and they are presented here only to serve as part of the introduction of the title material.

metamagnetic transition was attributed to magnetic domains [34] that disappear above T_M according to magneto-optical imaging and scanning Hall probe measurements [36]. On the other hand, the magnetic-field dependence of the bulk heat capacity does exhibit abrupt changes at the metamagnetic transition H_c, suggesting the metamagnetic behavior is not due to domains [37]. In addition, a rapid increase in the c-axis lattice parameter below T_M at ambient conditions is observed [35], signaling a critical role for strong spin-lattice coupling in determining the magnetic state. A similar conclusion is also drawn from studies of Raman scattering [14] and Ca- and La-doping behavior of $Sr_4Ru_3O_{10}$ [38]. A recent magnetic and transport study of nanoscale flakes (30–350 nm) of $Sr_4Ru_3O_{10}$ revealed a drastic size effect in the evolution from c-axis FM to a basal-plane AFM state [39]. In short, it is increasingly clear that spin-lattice coupling is critical to the apparent coexistence of the interlayer FM and the intralayer metamagnetism.

Application of pressure is a powerful tool for tuning lattice properties without introducing disorder, and should provide insights into the complex behavior of $Sr_4Ru_3O_{10}$. This work reports measurements of the magnetic and transport properties of bulk single-crystal $Sr_4Ru_3O_{10}$ at pressures up to 25 kbar in applied magnetic fields up to 14 T. Here, we report a rapid evolution from c-axis itinerant FM at ambient pressure to basal-plane itinerant AFM at pressures near 25 kbar, accompanied by a vanishing magnetic anisotropy that promotes the metamagnetic state at ambient pressure. This study indicates an unusually large magnetoelastic coupling operates in $Sr_4Ru_3O_{10}$, which makes it an ideal model system for studies of competing itinerant FM, AFM, and metamagnetism.

II. EXPERIMENTAL DETAILS

Single crystals of $Sr_4Ru_3O_{10}$ were grown using a self-flux method from off-stoichiometric quantities of RuO_2, $SrCO_3$, and $SrCl_2$. The average sample size is approximately $1 \times 1 \times 0.4$ mm^3. Measurements of crystal structures were performed using a Bruker D8 Quest ECO single-crystal diffractometer equipped with a PHOTON 50 complementary metal oxide semiconductor detector. Chemical analyses of the samples were performed using a combination of a Hitachi MT3030 Plus scanning electron microscope and an Oxford energy-dispersive x-ray spectroscope (EDX). Standard four-lead measurements of the electrical resistivity were carried out using a Quantum Design (QD) Dynacool PPMS system equipped with a 14-Tesla magnet. Magnetic properties were measured using a QD MPMS-7 superconducting quantum interference device magnetometer. Two hydrostatic pressure cells compatible with the QD instruments were used for measurements of electrical resistivity (up to 27 kbar) and magnetization (up to 13 kbar).

III. RESULTS AND DISCUSSION

$Sr_4Ru_3O_{10}$ has an orthorhombic structure with a *Pbam* space group, and room-temperature lattice parameters $a = 5.4982$ Å, $b = 5.4995$ Å, and $c = 28.5956$ Å [12]. One important structural detail is that in the outer two perovskite layers, the RuO_6 octahedra are rotated 5.25° about the c axis, whereas in the middle layer they are rotated 10.6° about the c axis in the *opposite direction* (see Fig. 1 inset) [12]. This structural feature has significant implications for the spin configuration and physical properties discussed below, due to the action of strong spin-lattice coupling [20].

It is established that the spins are ferromagnetically aligned along the c axis in $Sr_4Ru_3O_{10}$ at ambient conditions, effectively forming FM chains along the c axis, the easy axis [14,34,35]. (Note that Ref. [14] indicates a slight spin canting toward the basal plane at ambient pressure.) Our magnetic data indicate that application of a modest pressure readily destabilizes the c-axis FM state and fosters emergent AFM correlations with spins primarily aligned within the basal plane below T_M, as illustrated in Fig. 2. (Note the applied magnetic field is merely 0.1 T.) The pressure-induced change in T_M is clearly identified by the shift of a corresponding peak in the basal-plane magnetization M_{ab} and indicates an astonishing fourfold enhancement of M_{ab} as the applied pressure P increases from 0 to 10 kbar [Fig. 2(a)], whereas the c-axis magnetization M_c undergoes a comparable reduction [Fig. 2(b)]. A peak in M_c emerges at around P = 8 kbar and becomes well defined at $P = 10$ kbar. The occurrence of peaks in both M_{ab} and M_c at $P = 10$ kbar serve as a clear indication that an AFM ordered

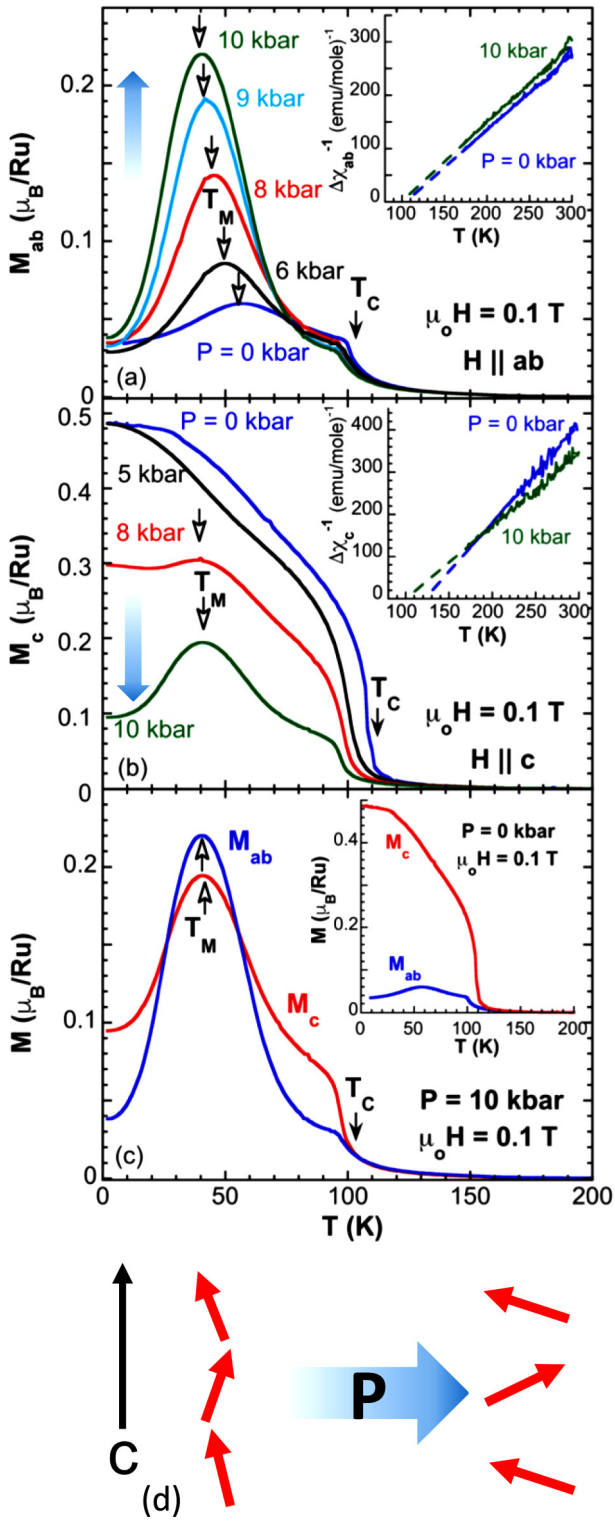

FIG. 2. Temperature dependence of the magnetization M at $\mu_o H = 0.1$ T for (a) the basal plane M_{ab}, (b) the c-axis M_c at representative pressures, and (c) M_{ab} and M_c at $P = 10$ kbar for comparison. Insets in (a) and (b): $1/\Delta\chi$ at $P = 0$ and 10 kbar vs T, where $\Delta\chi$ = magnetic susceptibility χ–Pauli susceptibility χ_o, for the basal plane and the c axis, respectively. Inset in (c): M_{ab} and M_c at $P = 0$ kbar. (d) Schematic for pressure-induced changes in the spin configuration. Note that the magnitude of M_{ab} (and M_c) rapidly increases (decreases) with P, which is highlighted by the two broad vertical arrows.

state is emerging [Fig. 2(c)]. Note that the observed anisotropy in M_{ab} and M_c, which at $P = 0$ kbar is 1 order of magnitude [Fig. 2(c) inset], almost vanishes near $P = 10$ kbar. In addition, the signature step in M_c at T_C decreases with P (see discussion below). This is consistent with a decrease in the Curie-Weiss temperature, θ_{cw}, under pressure that is illustrated in plots of $1/\Delta\chi$ ($\Delta\chi$ = magnetic susceptibility χ–Pauli susceptibility χ_o) for the basal plane and the c axis, respectively [insets in Figs. 2(a) and 2(b)]. As seen, θ_{cw} (intercept on the horizontal axis) changes from 122 K (105 K) at $P = 0$ kbar to 100 K (98 K) at 10 kbar for the c axis (the basal plane), suggesting a change in the exchange interaction due to application of pressure. Overall, applied pressure rapidly drives the magnetic state from a c-axis FM state toward a basal-plane AFM state below T_M. It is striking that a mere 10 kbar can cause such drastic changes in the magnetization and easy direction, which demonstrates an unusually strong magnetoelastic effect is at play in this material.

A Raman study of $Sr_4Ru_3O_{10}$ revealed a strong spin-phonon coupling of 5.2 cm^{-1} below T_M [14]. We infer that the pressure-induced AFM state is likely a result of a flattening of the RuO_6 octahedra, in which d_{xy} orbitals have the lowest energy and are fully occupied, whereas the d_{xz} and d_{yz} orbitals are half-filled. Superexchange interactions mediated by electrons in the d_{xz} and d_{yz} orbitals favor an AFM state [Fig. 2(d)], according to electronic band structure calculations [6,18,40]. This scenario also explains our observation of an unusual increase in the c-axis resistivity ρ_c with P at $T > T_C$, as shown in Fig. 3. The basal-plane resistivity ρ_{ab} changes only slightly with P, showing a small decrease with P at higher temperatures, presumably as a result of band broadening [Fig. 3(a)]. The slight change in ρ_{ab} implies that soft-phonon and spin-disorder scattering within the basal plane are largely unaffected under the conditions studied here. In sharp contrast, the c-axis resistivity ρ_c increases by a factor of 2 at $T > T_C$ [Fig. 3(b)]; in particular, the ratio of ρ_c/ρ_{ab} at 300 K rises from 3.8 at ambient pressure to 7.2 at 25 kbar [Fig. 3(a) inset]. Although a structural study of this compound under pressure is not yet available for a more conclusive discussion, tilting angle affects the orbital overlap, and qualitative and quantitative changes in resistivity are possible in general. The behavior demonstrated in Fig. 3 seems to suggest that applied pressure induces a tilting of the RuO_6 octahedra along the c axis, which reduces the Ru-O-Ru bond angle from 180° [Fig. 3(d)], which, in turn, reduces the overlap of p and d orbitals. This might help explain the significant increase in ρ_c for $T > T_C$ [Fig. 3(b)], and is also consistent with an anomalous pressure dependence of the 380-cm^{-1} B_{1g} phonon mode at low temperatures, which is attributed to a buckling of the RuO_6 octahedra [14]. Interestingly, the magnitude of ρ_c for $T < T_M$ is much less affected by applied pressure [Fig. 3(b)]. The rapidly reduced ρ_c below T_M signifies a strengthened overlap of d_{xz}/d_{yz} orbitals, and, more importantly, the existence of long-range magnetic order at $P = 25$ kbar; this is because electrical transport is intimately coupled to the magnetism, and long-range order significantly reduces both phonon and spin scattering.

Also of interest is the temperature dependence of $\rho_c \sim T^\alpha$ at low temperatures (1.8−10 K), where the exponent α changes significantly from near 2 at ambient pressure to

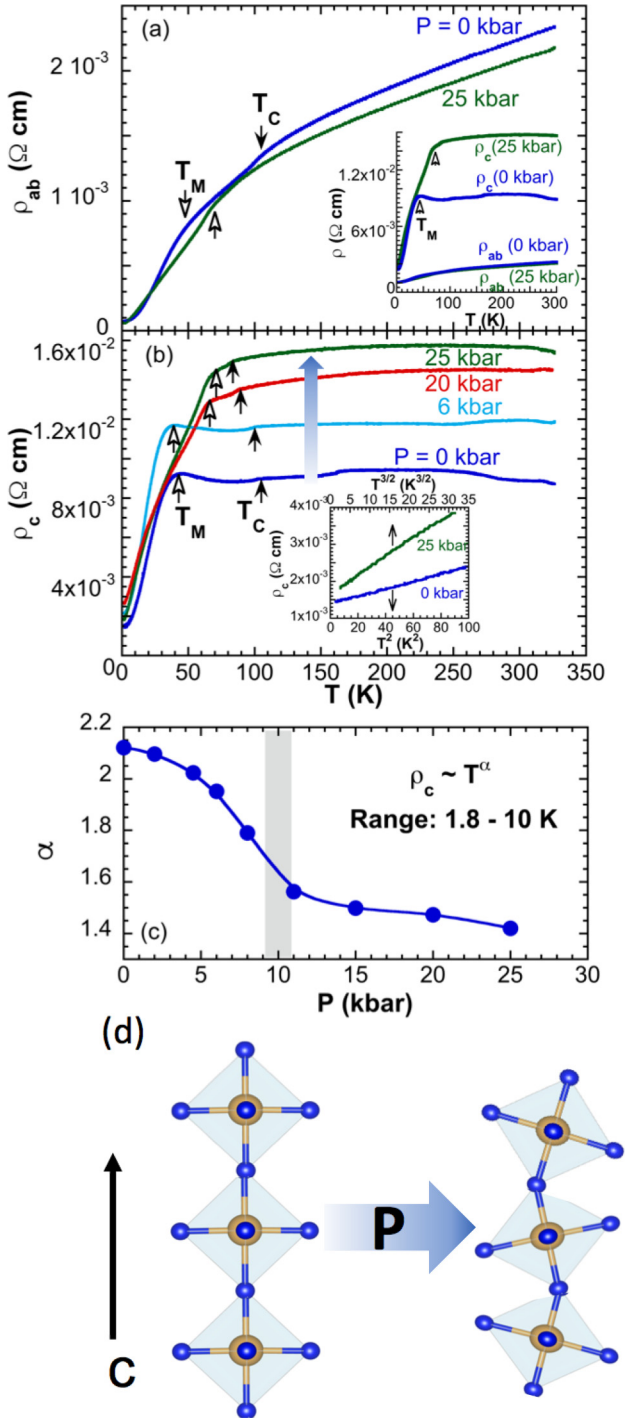

FIG. 3. Temperature dependence of the electrical resistivity for (a) the basal plane ρ_{ab} and (b) the c axis ρ_c at representative pressures. Note the modest decrease in ρ_{ab} and the considerable increase in ρ_c with P, which is marked by the broad arrow. (c) The exponent α of $\rho_c \sim T^\alpha$ as a function of pressure P. Note that the shaded area marks the rapid change in α. (d) Schematic for pressure-induced changes in the RuO_6 octahedra.

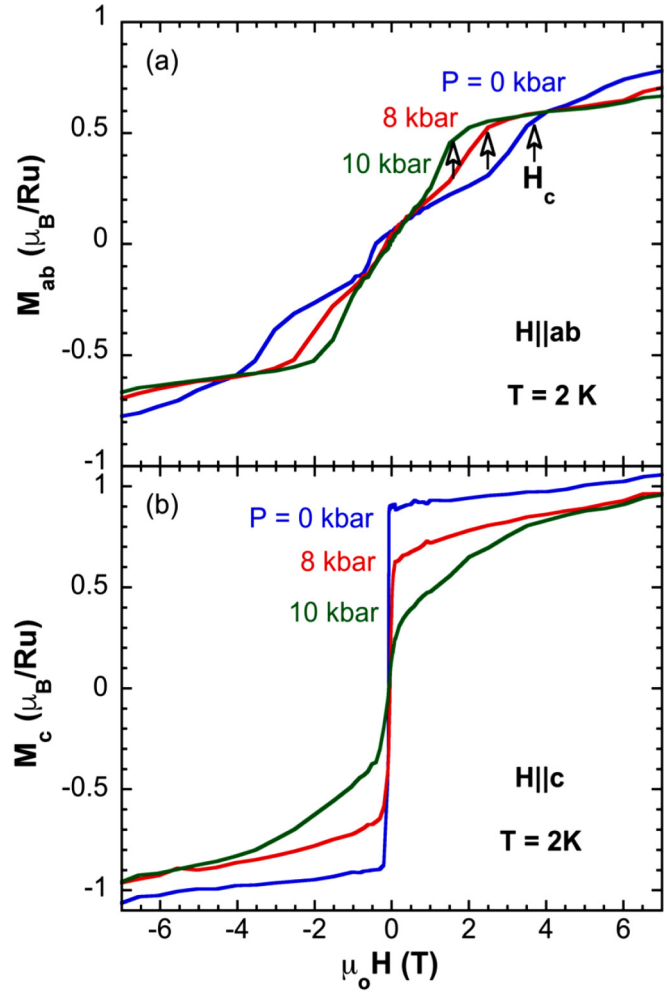

FIG. 4. The isothermal magnetization at $T = 2$ K for (a) the basal plane M_{ab} for $H||$ basal plane and (b) the c axis M_c for $H||c$ axis at a few representative pressures.

3/2 [see Fig. 3(b) inset], which suggests a dominance of AFM spin fluctuations and a breakdown of the Fermi liquid model [24]. As shown in Fig. 3(c), the value of α changes more rapidly near $P = 10$ kbar, which may mark an onset of a more isotropic itinerant AFM state [24]. The change in exponent α is correlated with changes of T_M, which increases at $P \geqslant 10$ kbar, while T_C steadily decreases over the same range [Fig. 3(b) shows ρ_c at a few representative pressures]. The opposite response of T_M and T_C to P further confirms that the basal-plane AFM state becomes more energetically favorable than the c-axis FM state with increasing distortion of the RuO_6 octahedra with increasing P. The data in Fig. 3 imply that the emergent basal-plane AFM state is dominant at $P \geqslant 10$ kbar.

The evolution of both the basal-plane and c-axis isothermal magnetizations at low temperatures also indicates that applied pressure enhances M_{ab} and weakens M_c, as shown in Fig. 4. The critical field of the metamagnetic transition H_c decreases with increasing P, indicative of an increasingly weakened magnetic anisotropy [Fig. 4(a)]. Note that magnetic field applied along the c axis helps elongate the RuO_6 octahedra along the c axis [14], thus enhancing M_c. This effect competes with applied pressure that tends to compress the RuO_6 octahedra. The result of the two competing effects may explain why M_c changes only modestly with P [Fig. 4(b)]. [Note that M_c in Fig. 2(b) was taken at a low

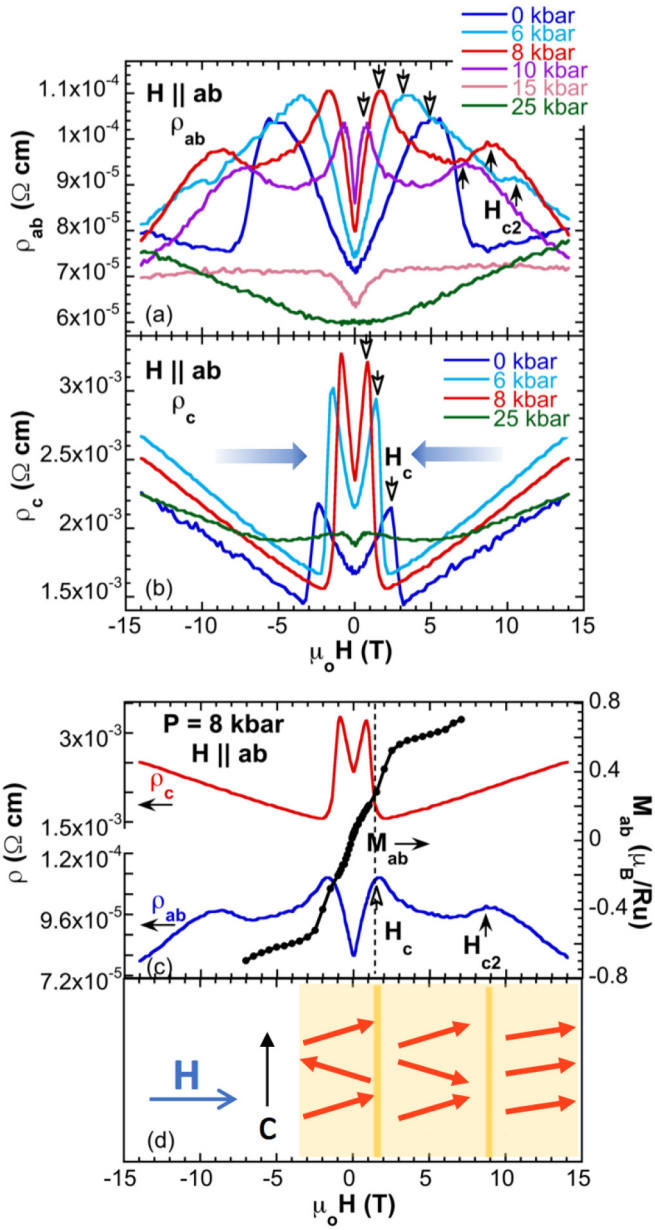

FIG. 5. Magnetic-field dependence of the electrical resistivity at 2 K for (a) the basal plane ρ_{ab}, (b) the c axis ρ_c at representative pressures, and (c) ρ_{ab} and ρ_c and M_{ab} (right scale) at $P = 8$ kbar for comparison. (d) Schematic for field-induced changes in the spin configuration. Note that the two broad horizontal arrows in Fig. 5(b) are to highlight the rapid decrease in H_c with P, and the vertical dashed line in Fig. 5(c) indicates H_c.

field, 0.1 T, where the field effect is negligible.] Moreover, both M_{ab} and M_c exhibit a sizable hysteresis effect at ambient pressure (Fig. 1) [12], but this hysteresis almost vanishes at $P = 10$ kbar (not shown), consistent with a weakened FM state.

The system exhibits a large negative magnetoresistivity $\rho(H)$ with an overall reduction of up to 80% (Fig. 5). [Note (1) that H is applied within the basal plane for both ρ_{ab} and ρ_c and (2) the data in Fig. 5 were taken at 2 K.] We propose that the basal-plane resistivity $\rho_{ab}(H)$ rises initially due to the canted AFM state, and then drops abruptly when H is strong enough to align the spins in a collinear fashion, which reduces spin scattering. Specifically, ρ_{ab} shows two peaks near two critical fields, H_c and H_{c2}, respectively. The peak at H_c marks the metamagnetic transition that signals a spin-flip (presumably in the middle layer) that aligns the middle layer spins with those in the outer layers; therefore all spins, although canted, are approximately polarized along with the direction of H, which reduces spin scattering and explains the abrupt drop in ρ_{ab} near H_c [Fig. 5(a)]. This is then followed at higher fields by another drop in ρ_{ab} at H_{c2} [Figs. 5(a) and 5(c)], which is already apparent but not well defined in M_{ab} in Fig. 4(a). It indicates an additional spin alignment which eventually diminishes the spin canting and further reduces spin scattering. The evolution of the spin configuration with H is schematically illustrated in Fig. 5(d). Note that ρ_c drops even more sharply near H_c but exhibits no anomaly at H_{c2}; it instead increases linearly with H when $H > H_c$ [Figs. 5(b) and 5(c)]. Since the direction of H is perpendicular to the direction of electrical current, the linear rise of ρ_c with H could be a result of the familiar deflection (orbital magnetoresistance) of electrons by the Lorentz force. On the other hand, this linear field dependence is strikingly similar to that observed in $Ca_3Ru_2O_7$, which is attributed to an orbital order that strengthens with increasing magnetic field, which hinders electron hopping [41,42]. The two critical fields H_c and H_{c2} rapidly decrease with increasing P and eventually vanish at $P = 25$ kbar, where $\rho_{ab} \sim H^2$ (ρ_c behaves similarly above 1 T). This trend is also evident in M_{ab} and M_c in Fig. 4. If an orbital order does indeed exist here, it is substantially weakened at 25 kbar [Fig. 5(b)].

It needs to be pointed out that the field dependences of both ρ_{ab} and ρ_c bear a strong resemblance to the *bulk spin-valve effect* observed in bilayered $Ca_3(Ru_{1-x}Cr_x)_2O_7$, which originates from inhomogeneous exchange coupling and soft and hard bilayers having antiparallel spin alignments [43]. Consistently, the distinct behavior demonstrated by ρ_{ab} and ρ_c (including somewhat different H_c) [Figs. 5(a)–5(c)] implies a strong exchange anisotropy that must arise from the competition between FM and AFM correlations. The anisotropy and spin-valve effect are clearly highly susceptible to the applied pressure and eventually vanish when P is greater than 25 kbar.

IV. CONCLUSIONS

A temperature-pressure phase diagram can be generated using the results of this study, as shown in Fig. 6. The lattice distortions destabilize the c-axis FM state, and foster a basal-plane AFM state (Figs. 2 and 4). As a result, T_C decreases at a rate $dT/dP \approx -1$ K/kbar, whereas T_M, which defines the onset of the AFM state, decreases initially and then rises for $P \gtrsim 10$ kbar (Figs. 2 and 3). Indeed, the rapid change in the temperature dependence of ρ_c (and ρ_{ab}) from T^2 to $T^{3/2}$ below 10 K near $P = 10$ kbar marks a crossover from the c-axis FM state to a predominantly basal-plane AFM state [Fig. 3(c)]. Nevertheless, the opposite pressure responses of T_C and T_M point to a merging of the two magnetic states at $P \gtrsim 25$ kbar, at which a collinear, itinerant AFM

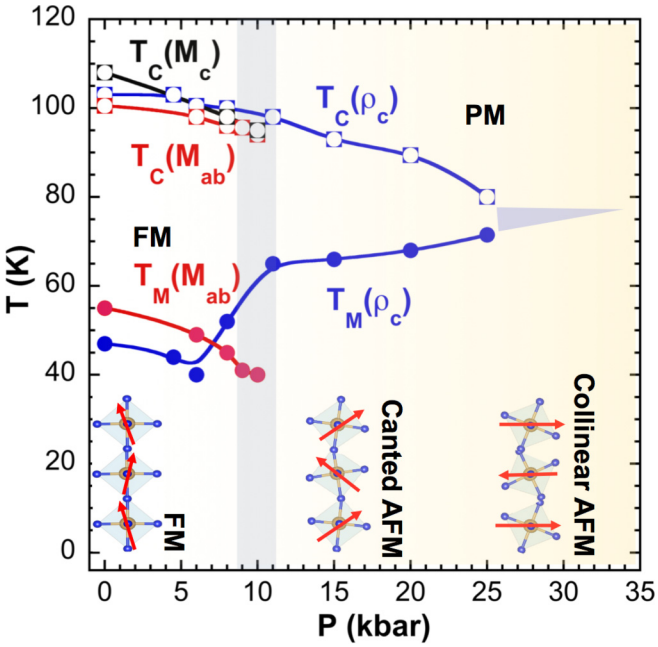

FIG. 6. A T-P phase diagram generated based on the magnetic and transport results. Note that T_C and T_M appear to merge as the antiferromagnetic state is fully developed at $P \geqslant 25$ kbar. Note that the shaded areas near 10 kbar mark a crossover from the c-axis FM state to a predominately basal-plane AFM state.

state is presumably fully established (Figs. 5 and 6). The existence of this pressure-induced long-range order at 25 kbar is strongly indicated by the abrupt drop in ρ_c below T_M [Figs. 3(a) inset and 3(b)]. We note that the attainment of a collinear antiferromagnetic state out of a low-pressure canted state should also generate a strongly varying anomalous (topological) Hall effect due to variations in the scalar spin chirality [44].

It is remarkable that the FM state with $T_C = 165$ K in the sister compound $SrRuO_3$ decreases with pressure at a slower rate $dT/dP \approx -0.68\,\mathrm{K/kbar}$ and only vanishes in a much higher pressure range of 170–340 kbar, where a paramagnetic state emerges [45]. This sharply contrasts with the high tunability offered by pressure applied in $Sr_4Ru_3O_{10}$ and highlights the rich physics available for study in this peculiar layered magnet.

ACKNOWLEDGMENTS

G.C. is thankful to Dr. Mingliang Tian for useful discussions and to the High Magnetic Field Laboratory, Chinese Academy of Sciences, for the hospitality during which part of this paper was drafted. This work was supported by NSF Grant No. DMR-1712101, and the research of L.E.D. is supported by NSF Grant No. DMR-1506979.

[1] Y. Maeno, H. Hashingmoto, K. Yoshida, S. Ishizaki, T. Fujita, J. G. Bednorz, and F. Lichtenberg, Nature (London) **372**, 532 (1994).
[2] R. J. Cava, B. Batlogg, K. Kiyono, H. Takagi, J. J. Krajewski, W. F. Peck, Jr., L. W. Rupp, Jr., and C. H. Chen, Phys. Rev. B **49**, 11890 (1994).
[3] L. Klein, J. S. Dodge, C. H. Ahn, G. J. Snyder, T. H. Geballe, M. R. Beasley, and A. Kapitulnik, Phys. Rev. Lett. **77**, 2774 (1996).
[4] G. Cao, S. McCall, J. E. Crow, and R. P. Guertin, Phys. Rev. Lett. **78**, 1751 (1997).
[5] G. Cao, S. McCall, M. Shepard, J. E. Crow, and R. P. Guertin, Phys. Rev. B **56**, 321 (1997).
[6] I. I. Mazin and D. J. Singh, Phys. Rev. B **56**, 2556 (1997).
[7] G. Cao, S. McCall, M. Shepard, J. E. Crow, and R. P. Guertin, Phys. Rev. B **56**, R2916(R) (1997).
[8] S. I. Ikeda, Y. Maeno, S. Nakatsuji, M. Kosaka, and Y. Uwatoko, Phys. Rev. B **62**, R6089(R) (2000).
[9] R. S. Perry, L. M. Galvin, S. A. Grigera, L. Capogna, A. J. Schofield, A. P. Mackenzie, M. Chiao, S. R. Julian, S. I. Ikeda, S. Nakatsuji, Y. Maeno, and C. Pfleiderer, Phys. Rev. Lett. **86**, 2661 (2001).
[10] S. A. Grigera, R. P. Perry, A. J. Schofield, M. Chiao, S. R. Julian, G. G. Lonzarich, S. I. Ikeda, Y. Maeno, A. J. Millis, and A. P. Mackenzie, Science **294**, 329 (2001).
[11] Y. Maeno, T. M. Rice, and M. Sigrist, Phys. Today **54**, 42 (2001).
[12] M. K. Crawford, R. L. Harlow, W. Marshall, Z. Li, G. Cao, R. L. Lindstrom, Q. Huang, and J. W. Lynn, Phys. Rev B **65**, 214412 (2002).
[13] X. N. Lin, Z. X. Zhou, V. Durairaj, P. Schlottmann, and G. Cao, Phys. Rev. Lett. **95**, 017203 (2005).
[14] R. Gupta, M. Kim, H. Barath, S. L. Cooper, and G. Cao, Phys. Rev. Lett. **96**, 067004 (2006).
[15] Z. Q. Mao, M Zhou, J. Hooper, V. Golub, and C. J. O'Connor, Phys. Rev. Lett. **96**, 077205 (2006).
[16] R. G. Moore, Jiandi Zhang, V. B. Nascimento, R. Jin, Jiandong Guo, G. T. Wang, Z. Fang, D. Mandrus, and E. W. Plummer, Science **318**, 615 (2007).
[17] R. G. Moore, V. B. Nascimento, Jiandi Zhang, J. Rundgren, R. Jin, D. Mandrus, and E. W. Plummer, Phys. Rev. Lett. **100**, 066102 (2008).
[18] M. Malvestuto, E. Carleschi, R. Fittipaldi, E. Gorelov, E. Pavarini, M. Cuoco, Y. Maeno, F. Parmigiani, and A. Vecchione, Phys. Rev. B **83**, 165121 (2011).
[19] R. Jin, in *Frontiers of 4d- and 5d- Transition Metal Oxides*, edited by G. Cao and L. E. De Long (World Scientific, London, 2013), Chap. 5.
[20] G. Cao, L. E. DeLong, and P. Schlottmann, in *Frontiers of 4d- and 5d- Transition Metal Oxides*, edited by G. Cao and L. E. De Long (World Scientific, London, 2013), Chap. 6.
[21] G. Cao, L. Balicas, W. H. Song, Y. P. Sun, Y. Xin, V. A. Bondarenko, J. W. Brill, S. Parkin, and X. N. Lin, Phys. Rev. B **68**, 174409 (2003).
[22] Y. J. Jo, L. Balicas, N. Kikugawa, E. S. Choi, K. Storr, M. Zhou, and Z. Q. Mao, Phys. Rev. B **75**, 094413 (2007).
[23] E. Carleschi, B. P. Doyle, R. Fittipaldi, V. Granata, A. M. Strydom, M. Cuoco, and A. Vecchione, Phys. Rev. B **90**, 205120 (2014).

[24] T. Moriya, *Spin Fluctuations in Itinerant Electron Magnetism* (Springer-Verlag, Berlin, 1985).
[25] P. Fazekas, *Lecture Notes on Electron Correlation and Magnetism* (World Scientific, London, 1999).
[26] E. C. Stoner, Proc. R. Soc. London A **165**, 372 (1938).
[27] E. P. Wohlfarth and P. Rhodes, Philos. Mag. **7**, 1817 (1962).
[28] H. Yamada, Phys. Rev. B **47**, 11211 (1993).
[29] B. Binz and M. Sigrist, Europhys. Lett. **65**, 816 (2004).
[30] C. Mirri, F. M. Vitucci, P. Di Pietro, S. Lupi, R. Fittipaldi, V. Granata, A. Vecchione, U. Schade, and P. Calvani, Phys. Rev. B **85**, 235124 (2012).
[31] M. Malvestuto, V. Capogrosso, E. Carleschi, L. Galli, E. Gorelov, E. Pavarini, R. Fittipaldi, F. Forte, M. Cuoco, A. Vecchione, and F. Parmigiani, Phys. Rev. B **88**, 195143 (2013).
[32] Y. Liu, W. Chu, J. Yang, G. Liu, H. Du, W. Ning, L. Ling, W. Tong, Z. Qu, G. Cao, Z. Xu, and M. Tian, Phys. Rev. B **98**, 024425 (2018).
[33] F. Weickert, L. Civale, B. Maiorov, M. Jaime, M. B. Salamon, E. Carleschi, A. M. Strydom, R. Fittipaldi, V. Granata, and A. Vecchione, Sci. Rep. **7**, 3867 (2017).
[34] W. Bao, Z. Q. Mao, M. Zhou, J. Hooper, J. W. Lynn, R. S. Freitas, P. Schiffer, Y. Liu, H. Q. Yuan, and M. Salamon, arXiv:cond-mat/0607428.
[35] V. Granata, L. Capogna, M. Reehuis, R. Fittipaldi, B. Ouladdiaf, S. Pace, M. Cuoco, and A. Vecchione, J. Phys.: Condens. Matter **25**, 056004 (2013).
[36] Y. Nakajima, Y. Matsumoto, D. Fobes, M. Zhou, Z. Q. Mao, and T. Tamegai, J. Phys.: Conf. Ser. **150**, 042134 (2009).
[37] G. Cao, S. Chikara, J. W. Brill, and P. Schlottmann, Phys. Rev. B **75**, 024429 (2007).
[38] S. Chikara, V. Durairaj, W. H. Song, Y. P. Sun, X. N. Lin, A. Douglass, G. Cao, P. Schlottmann, and S. Parkin, Phys. Rev. B **73**, 224420 (2006).
[39] Y. Liu, J. Yang, W. Wang, H. Du, W. Ning, L. Ling, W. Tong, Z. Qu, Z. Yang, M. Tian, G. Cao, and Y. Zhang, New J. Phys. **18**, 053019 (2016).
[40] M. Cuoco, F. Forte, and C. Noce, Phys. Rev. B **73**, 094428 (2006).
[41] G. Cao, X. N. Lin, L. Balicas, S. Chikara, J. E. Crow, and P. Schlottmann, New J. Phys. **6**, 159 (2004), Special Issue on Orbital Physics.
[42] G. Cao, L. Balicas, X. N. Lin, S. Chikara, E. Elhami, V. Duairaj, J. W. Brill, R. C. Rai, and J. E. Crow, Phys. Rev. B **69**, 014404 (2004).
[43] G. Cao, V. Durairaj, S. Chikara, L. E. DeLong, and P. Schlottmann, Phys. Rev. Lett. **100**, 016604 (2008).
[44] L. Shlyk, S. Parkin, and L. E. De Long, Phys. Rev. B **81**, 014413 (2010).
[45] J. J. Hamlin, S. Deemyad, J. S. Schilling, M. K. Jacobsen, R. S. Kumar, A. L. Cornelius, G. Cao, and J. J. Neumeier, Phys. Rev. B **76**, 014432 (2007).